

Interference effect on the liquid-crystal-based Stokes polarimeter

Jun-Feng Hou(侯俊峰)[1,2,†], Dong-Guang Wang(王东光)[1], Yuan-Yong Deng(邓元勇)[1,2], Zhi-Yong Zhang(张志勇)[1,2], and Ying-Zi Sun(孙英姿)[1]

Citation: Chin. Phys. B, 2020, 29 (**12**): 124211. DOI: 10.1088/1674-1056/abbbf4
Journal homepage: http://cpb.iphy.ac.cn; http://iopscience.iop.org/cpb

What follows is a list of articles you may be interested in

Irradiation study of liquid crystal variable retarder for Full-disk Magneto-Graph payload onboard ASO-S mission

Jun-Feng Hou(侯俊峰), Hai-Feng Wang(王海峰), Gang Wang(王刚), Yong-Quan Luo(骆永全), Hong-Wei Li(李宏伟), Zhen-Long Zhang(张振龙), Dong-Guang Wang(王东光), Yuan-Yong Deng(邓元勇)
Chin. Phys. B, 2020, 29 (**7**): 074208. DOI: 10.1088/1674-1056/ab8c40

Dynamic manipulation of probe pulse and coherent generation of beating signals based on tunneling-induced inference in triangular quantum dot molecules

Nuo Ba(巴诺), Jin-You Fei(费金友), Dong-Fei Li(李东飞), Xin Zhong(钟鑫), Dan Wang(王丹), Lei Wang(王磊), Hai-Hua Wang(王海华), Qian-Qian Bao(鲍倩倩)
Chin. Phys. B, 2020, 29 (**3**): 034204. DOI: 10.1088/1674-1056/ab683d

Dynamic properties of atomic collective decay in cavity quantum electrodynamics

Yu-Feng Han(韩玉峰), Cheng-Jie Zhu(朱成杰), Xian-Shan Huang(黄仙山), Ya-Ping Yang(羊亚平)
Chin. Phys. B, 2018, 27 (**12**): 124206. DOI: 10.1088/1674-1056/27/12/124206

Physical manipulation of ultrathin-film optical interference for super absorption and two-dimensional heterojunction photoconversion

Guo-Yang Cao(曹国洋), Cheng Zhang(张程), Shao-Long Wu(吴绍龙), Dong Ma(马冬), Xiao-Feng Li(李孝峰)
Chin. Phys. B, 2018, 27 (**12**): 124202. DOI: 10.1088/1674-1056/27/12/124202

Two-dimensional atom localization induced by a squeezed vacuum

Fei Wang(王飞), Jun Xu(徐俊)
Chin. Phys. B, 2016, 25 (**10**): 104201. DOI: 10.1088/1674-1056/25/10/104201

Interference effect on the liquid-crystal-based Stokes polarimeter*

Jun-Feng Hou(侯俊峰)[1,2,†], Dong-Guang Wang(王东光)[1], Yuan-Yong Deng(邓元勇)[1,2], Zhi-Yong Zhang(张志勇)[1,2], and Ying-Zi Sun(孙英姿)[1]

[1] *Key Laboratory of Solar Activity, National Astronomical Observatories, Chinese Academy of Sciences, Beijing* 100101, *China*
[2] *School of Astronomy and Space Science, University of Chinese Academy of Sciences, Beijing* 101408, *China*

(Received 23 July 2020; revised manuscript received 9 September 2020; accepted manuscript online 28 September 2020)

The Stokes polarimeter based on liquid crystal variable retarders (LCVRs) is envisaged as a promising novel technique for polarization measurement in space applications due to the inherent advantage of eliminating the need for conventional rotating polarizing optics and increasing the measuring speed. However, the intrinsic multi-beam interference in LCVRs limits its polarization accuracy by several percent. How to eliminate the influence of the interference effect becomes an urgent issue for the liquid-crystal-based Stokes polarimeter. The present study introduces a simplified but effective interference model based on the thin-film optics and polarized light theory to simulate the relationship between the interference effect of the LCVRs-based Stokes polarimeter and the polarization accuracy. The simulation results show that the transmittance variation of LCVR with the derived voltage is caused by multi beam interference between the indium tin oxide (ITO) film and the liquid crystal within LCVR, which produces a few percent of instrumental polarization. The instrumental polarization is about 0.01 and different for different wavelengths. An optimization method was proposed to reduce the instrumental polarization to 0.002, effectively improving the polarization sensitivity of the Stokes polarimeter limited by the interference. In addition, an experimental setup was built up to measure and analyze the influence of the interference effect of the LCVRs-based Stokes polarimeter on the polarization accuracy before and after the optimization. The experiment results are in good agreement with the simulation.

Keywords: polarimetry, liquid crystal variable retarder (LCVR), interference effect

PACS: 42.70.Df, 95.75.Hi, 95.55.Qf, 95.55.Ev **DOI:** 10.1088/1674-1056/abbbf4

1. Introduction

The primary physical quantities associated with an electromagnetic wave (optical field) are intensity, wavelength, coherence, and polarization. Conventional panchromatic cameras measure the intensity of optical radiation over a particular waveband of interest. Spectral imagers measure the intensity in several wavebands, which can range from one or two (three is common for a color camera), through multispectral to hyperspectral systems.[1] In the case of remote sensing, spectral sensors give us information about the distribution of material components in a sample;[2,3] polarimetry provides information about the surface features, shape, shading, and roughness.[4–6] In astronomy, spectroscopic measurements yield details about the temperature, density, and Doppler velocity, whereas, polarimetry gives details on other physical parameters such as magnetic fields and electric fields.[7–9] Polarization provides more information than spectral and intensity images, and thus plays an essential role in remote sensing and astronomy.

A standard Stokes polarimeter consists of a modulator and an analyzer for measuring the polarization signals. Presently, especially in the visible light range, many modulation schemes are employed to built polarimeters and measure the full Stokes vector, for example, mechanical modulation, photo-elastic modulation (PEM), potassium dideuterium phosphate (KD*P) modulation, liquid crystal variable retarders (LCVRs) modulation, and ferro-electric liquid crystal retarders (FeLCs) modulation.[10–18] In space applications, photo-elastic modulation is seldom used in imaging polarization measurement due to its ultra-high modulation frequency (dozens of kHz); KD*P modulations are complex and difficult to be used in space because of high AC voltage and material characteristic. Mechanical modulation is the most classical modulation method, which realizes polarization measurement by rotating a polarizer or a retarder. However, the slow modulation speed and risk of rotating mechanism limit its scope of use in high sensitivity polarimetry in space-based instruments. In contrast, LCVR modulation is envisaged as a promising novel technique for a polarization instrument onboard a spacecraft due to its inherent advantage of eliminating the need for conventional rotary polarizing optics and thus increasing the measuring speed.

LCVRs were used as polarization modulators for the first time in an aerospace mission which was attempted by the Flare Generis mission.[19] The Flare Genesis Experiment was a balloon-borne spectro-polarimeter which aimed at obtaining the vector-magnetograms of the solar photosphere and chromosphere. Many of the technologies derived from the Flare Genesis Experiment were later used in the successful IMaX

*Project supported by the Strategic Pioneer Program on Space Science, Chinese Academy of Sciences (Grant Nos. XDA15010800 and XDA15320102) and the National Natural Science Foundation of China (Grant Nos. 11427901, 11773040, 11403047, and 11427803).

†Corresponding author. E-mail: jfhou@bao.ac.cn

© 2020 Chinese Physical Society and IOP Publishing Ltd

instrument of the Sunrise mission.[20,21] Another application of LCVRs in space is in Solar Orbiter,[22] a mission of the Cosmic Vision program of the European Space Agency (ESA) and was launched in 2020. The objective of this space mission is to observe the sun, using a suite of advanced scientific instruments and at an approach point to the sun as close as 0.28 AU during part of its orbit. There are two payloads, the polarimetric and helioseismic imager (SO/PHI) and the multi-element telescope for imaging and spectroscopy (METIS)[23] which use LCVRs as modulators. Also, the full-disk magnetograph (FMG),[24] one of the payloads onboard the Advanced Space Solar Observatory (ASO-S),[25] uses LCVRs as the polarization modulators. ASO-S mission is specifically proposed to understand the physical processes involved in solar flares, CMEs, and the solar magnetic field evolution, scheduled to be launched in 2021.

However, the interference effect is a severe problem that one must address in the LCVRs-based Stokes polarimeter. The effective thickness (optical path) of the liquid crystal layer in LCVR is of the same order of the observing wavelength, which makes it easier for the multi-beam interference to occur due to the refractive index mismatch in LCVR. Consequently, how to analyze, forecast, optimize, and reduce the influence of the interference effect on the polarization accuracy becomes an urgent issue for the use of LCVRs-based Stokes polarimeter with high accuracy.

This paper introduces a simplified but effective interference model based on the thin-film optics and polarized light theory, and simulates the relationship between the interference effect of the LCVRs-based Stokes polarimeter and polarization accuracy. An optimization method is proposed to reduce the instrumental polarization by effectively improving the polarization sensitivity of the Stokes polarimeter. An experiment was set up to measure and analyze the influence of the interference effect in the LCVRs-based Stokes polarimeter on the polarization accuracy. The remainder of this paper is organized as follows. Section 2 briefly reviews the design of LCVRs-based Stokes polarimeter. Section 3 builds a polarization model of LCVRs-based Stokes polarimeter with interference. Section 4 presents the simulation results and discusses the optimization method to reduce the instrumental polarization. Section 5 gives the experimental datasets and results as well as the detailed analyses, and discusses some issues. Finally, Section 6 concludes the paper.

2. LCVRs-based Stokes polarimeter

2.1. LCVR[26]

An LCVR consists of a nematic liquid-crystal (LC) material layer sandwiched between two fused-silica substrates (illustrated in Fig. 1). The outer surfaces of both substrates are coated with an antireflective film to reduce reflection. The inner surfaces of both substrates are coated with a transparent indium tin oxide (ITO) electrode and a polyimide layer in turn. Some spacers are used to control the thickness of the liquid crystal accurately. The polyimide layer forces an initial orientation of the LC molecules in a direction parallel to that of the silica plates, which defines the optics axis of LCVR. The application of a voltage through the ITO films generates a homogeneous electric field inside the cavity that forces the LC molecules to tilt to a given angle with respect to the substrate surface. Thus the birefringence index is changed, and the retardations of LCVR will vary with the voltages (shown in Fig. 2).[27] In other words, LCVR is an electro-optic modulator, and it can modulate the linear polarization to circular or vice versa by changing the voltage.

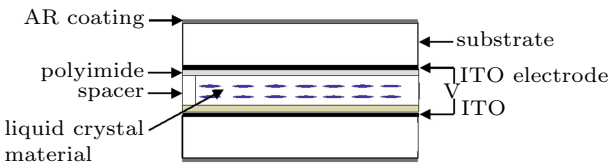


Fig. 1. The construction of LCVR.

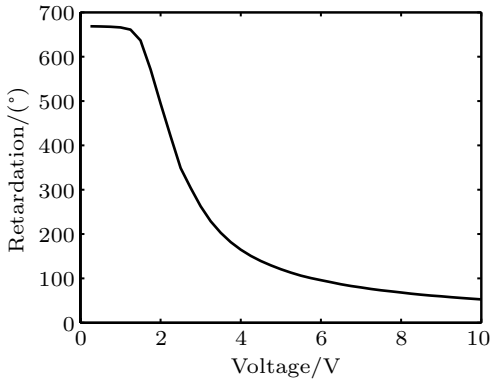


Fig. 2. The relations of retardation of LCVR with voltages.

2.2. Design of LCVRs-based Stokes polarimeter

Polarized light from an object is conventionally described through the Stokes vector, $\boldsymbol{S}_{\text{in}} = [I, Q, U, V]^{\text{T}}$, where I is the intensity, Q and U are two independent linear polarizations, and V is the circular polarization. In general, the Stokes vectors are measured by a Stokes polarimeter with a polarization modulator and a polarizer. The polarization modulator is used to realize the modulation among polarization signals (Stokes Q, U, and V), and the polarizer is used to modulate the polarization signals into the intensity (Stokes I). The combination modulation of polarization modulator and polarizer realizes the measurement of full Stokes parameters (I, Q, U, and V). In a LCVRs-based Stokes polarimeter, the polarization modulator consists of two liquid crystal variable retarders, LCVR1 and LCVR2 (as shown in Fig. 3). The fast axis orientation of the LCVR1 is the same as that of the polarizer (setting at 0°

in the horizontal direction). The angle between the fast axis orientations of LCVR2 and LCVR1 is 45°. The polarization modulator is driven by the application of voltages to LCVRs to convert the desired incoming polarization into the fixed linear polarization selected by the polarizer.

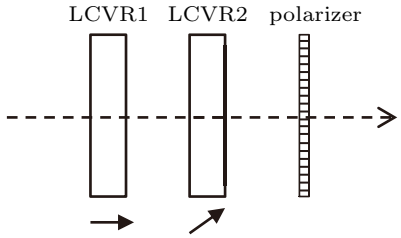


Fig. 3. Design of LCVRs-based Stokes polarimeter.

Table 1 gives a full modulation scheme of the LCVRs-based Stokes polarimeter to realize the measurement of Stokes vector $\boldsymbol{S}_{\rm in} = [I,Q,U,V]^{\rm T}$ from an object. Researchers can choose any combination of six states to measure the required parameters. For example, one can select the first four states to measure the linear polarization (which is common in remote sensing); also, one can choose the last two states to measure the circular polarization. All the six states are chosen to measure the full Stokes parameters, which is essential in the case of solar magnetic field measurement. Even though three intensity measurements are enough to determine the linear polarization and four intensity measurements are enough for the full Stokes parameters, more modulation stages have been selected for robustness reasons and simplicity in the later scientific data analysis.

Table 1. Modulation scheme of the LCVRs-based Stokes polarimeter. θ_1, θ_2 and δ_1, δ_2 are azimuth and retardation of both LCVRs, respectively. $\theta_{\rm p}$ is the azimuth of the polarizer.

States	θ_1	θ_2	$\theta_{\rm p}$	δ_1	δ_2	Modulated signal
1	0°	45°	0°	0°	0°	$0.5(I+Q)$
2	0°	45°	0°	0°	180°	$0.5(I-Q)$
3	0°	45°	0°	90°	90°	$0.5(I+U)$
4	0°	45°	0°	90°	270°	$0.5(I-U)$
5	0°	45°	0°	0°	90°	$0.5(I+V)$
6	0°	45°	0°	0°	270°	$0.5(I-V)$

3. Polarization model of LCVRs-based Stokes polarimeter with interference

3.1. Interference effect

Interference effects can be seen in most of the optical elements. However, it can be reduced or even eliminated by adding an anti-reflective (AR) coating on their outer surfaces. Therefore, the interference effect is often ignored while using some materials, such as glasses, crystal waveplate, MgF_2 crystal, but cannot be ignored in the case of LCVR. Table 2 lists the materials, refractive indexes, and thicknesses of a common LCVR we have used. It is found that the interference effect from ITO could not be ignored due to its large refractive index relative that of the liquid crystal, and the reflectivity is about 0.02 (calculated by Fresnel formula[28]). Furthermore, the liquid crystal has a larger birefringence index compared to other uniaxial crystals, which makes it challenging to eliminate the interference effect by using AR coating or refractive index matching. In addition, the effective extraordinary index $n_{\rm e}$ varies with the voltages applied to LCVR, which induces an additional interference effect. Thus, the interference becomes a significant problem that we have to face and deal with in LCVRs-based Stokes polarimeter.

Table 2. Materials, refractive index, and thickness in LCVR.

Material	Refractive index	Thickness
Fused silicon	$n_{\rm o} = 1.46$	5 mm
ITO	$n_{\rm o} = 2.0$	50 nm
Polyimide	$n_{\rm o} = 1.5$	300 nm
Liquid crystal	$n_{\rm o} = 1.5$, $n_{\rm e} = 1.76$	5 μm

3.2. Interference model of LCVR

As the interference mainly comes from the refractive index difference between ITO and liquid crystal, an LCVR can be further simplified to three-layer films: ITO, liquid crystal, and ITO. The simple model is shown in Fig. 4, where n_j and d_j represent the refractive index and thickness of the j-th layer.

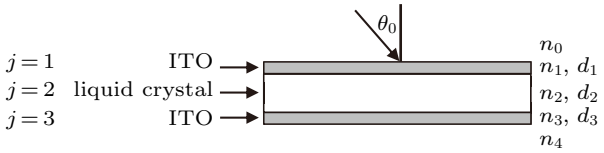


Fig. 4. The simplified geometric model of LCVR.

For an isotropic film as ITO, based on the theory of thin-film optics,[28] the interference effect of the j-th film can be described entirely by a characteristic matrix $\boldsymbol{M}_j$,

$$\boldsymbol{M}_j = \begin{bmatrix} \cos\delta_j & \dfrac{\rm i}{\eta_j}\sin\delta_j \\ {\rm i}\eta_j\sin\delta_j & \cos\delta_j \end{bmatrix}, \tag{1}$$

where δ_j and η_j are the retardation and effective refractive index of the j-th layer and can be calculated by

$$\delta_j = \frac{2\pi}{\lambda} n_j d_j \cos\theta_j, \tag{2}$$

$$\eta_j = \begin{cases} n_j\cos\theta_j, & \text{s-polarization}, \\ \dfrac{n_j}{\cos\theta_j}, & \text{p-polarization}. \end{cases} \tag{3}$$

Here λ is the measured wavelength, and θ_j is the refractive angle and can be derived by Snell's law. It is noted that η_j has different response for different (s- or p-) incident polarization when $\theta_j \neq 0$. Thus, $\boldsymbol{M}_j$ would be different for s- and p-polarization. But it is not the case for the uniaxial crystal as liquid crystal. However, the characteristic matrix Eq. (1) will still be available for liquid crystal if the principal plane of

the ray and the principal section of the liquid crystal coincide, when s-polarization and p-polarization coincide with the ordinary light and the extraordinary light, respectively. δ_j and η_j in Eq. (1) for liquid crystal are described by

$$\delta_j = \begin{cases} \dfrac{2\pi}{\lambda} n_{\rm o} d_j \cos\theta_j, & \text{s-polarization}, \\ \dfrac{2\pi}{\lambda} \bar{n}_{\rm e} d_j \cos\theta_j, & \text{p-polarization}, \end{cases} \tag{4}$$

$$\eta_j = \begin{cases} n_{\rm o}\cos\theta_j, & \text{s-polarization}, \\ \dfrac{\bar{n}_{\rm e}}{\cos\theta_j}, & \text{p-polarization}, \end{cases} \tag{5}$$

where $n_{\rm o}$ is the refractive index of the ordinary light, and $\bar{n}_{\rm e}$ is the effective refractive index of the extraordinary light. $\bar{n}_{\rm e}$ varies with the incident angle and voltages applied to LCVR and can be calculated by

$$\bar{n}_{\rm e} = \frac{n_{\rm o} n_{\rm e}}{\sqrt{n_{\rm o}^2 \cos^2(\theta_j+\beta) + n_{\rm e}^2 \sin^2(\theta_j+\beta)}}, \tag{6}$$

where β is the molecule tilt angle of the liquid crystal. To illustrate the characteristics of the tilt angle, we use a general expression for the molecule tilt angle of a liquid crystal as a function of the applied voltage,[29]

$$\beta = \begin{cases} 0, & V \leqslant V_{\rm c}, \\ \dfrac{\pi}{2} - 2\tan^{-1}\exp\left\{-\left(\dfrac{V-V_{\rm c}}{V_0}\right)^{0.55}\right\}, & V > V_{\rm c}, \end{cases} \tag{7}$$

where V is the applied voltage, $V_{\rm c}$ is a critical voltage at which the tilting process begins, and V_0 is the excess voltage.

3.3. Polarization model of LCVR with interference

The characteristic matrix $\boldsymbol{M}_j$ represents the relationship between electromagnetic fields on two adjacent interfaces of the j-th film,

$$\begin{bmatrix} E_{\rm j-1} \\ H_{j-1} \end{bmatrix} = \boldsymbol{M}_j \begin{bmatrix} E_{\rm j+1} \\ H_{j+1} \end{bmatrix}, \tag{8}$$

thus, the electromagnetic fields of the incident light and the outgoing light in LCVR have the following relations:

$$\begin{bmatrix} E_0 \\ H_0 \end{bmatrix} = \boldsymbol{M}_1\boldsymbol{M}_2\boldsymbol{M}_3 \begin{bmatrix} E_4 \\ H_4 \end{bmatrix} = \boldsymbol{M}_{\rm LCVR} \begin{bmatrix} E_4 \\ H_4 \end{bmatrix}. \tag{9}$$

According to the Maxwell equation and its boundary conditions, equation (9) is transformed into the following form:

$$\begin{bmatrix} E_{0,\rm i} + E_{0,\rm r} \\ (E_{0,\rm i} - E_{0,\rm r})\eta_0 \end{bmatrix} = \boldsymbol{M}_{\rm LCVR} \begin{bmatrix} E_{4,\rm t} \\ \eta_4 E_{4,\rm t} \end{bmatrix}, \tag{10}$$

where $E_{0,\rm i}$, $E_{0,\rm r}$, and $E_{4,\rm t}$ are respectively the amplitudes of the incident light, reflected light, and refracted light of the LCVR. Then the Fresnel coefficients, $t_{\rm s}$ and $t_{\rm p}$, can be obtained by

$$t_{\rm s,p} = \frac{E_{4,\rm t}}{E_{0,\rm i}}. \tag{11}$$

Correspondingly, the Mueller matrix of the LCVR for transmission can be calculated by

$$\boldsymbol{M}^{\rm t}_{\rm LCVR} = \frac{1}{2}\begin{bmatrix} A & B & 0 & 0 \\ B & A & 0 & 0 \\ 0 & 0 & C & D \\ 0 & 0 & -D & C \end{bmatrix}, \tag{12}$$

$$\begin{aligned} A &= |t_{\rm p}|^2 + |t_{\rm s}|^2, \\ B &= |t_{\rm p}|^2 - |t_{\rm s}|^2, \\ C &= 2{\rm Re}(t_{\rm p}^* t_{\rm s}), \\ D &= 2{\rm Im}(t_{\rm p}^* t_{\rm s}). \end{aligned} \tag{13}$$

$\boldsymbol{M}^{\rm t}_{\rm LCVR}$ represents the polarization model of the LCVR with interference. It describes the relations between the incident and outgoing Stokes vectors of the LCVR.

3.4. Polarization model of LCVRs-based Stokes polarimeter with interference

The total Mueller matrix $\boldsymbol{M}_{\rm s}$ of LCVRs-based Stokes polarimeter is the product of those of the polarizer, LCVR2, and LCVR1,

$$\boldsymbol{M}_{\rm s} = \tau \boldsymbol{M}_{\rm p} \boldsymbol{R}^{-1}_{45^\circ} \boldsymbol{M}^{\rm t}_{\rm LCVR2} \boldsymbol{R}_{45^\circ} \boldsymbol{M}^{\rm t}_{\rm LCVR1} \boldsymbol{S}_{\rm in}, \tag{14}$$

where τ is the total transmittance of the system; $\boldsymbol{M}^{\rm t}_{\rm LCVR1}$ and $\boldsymbol{M}^{\rm t}_{\rm LCVR2}$ are the Mueller matrices of LCVR1 and LCVR2, respectively; $\boldsymbol{R}_{45^\circ}$ is a rotation matrix; and $\boldsymbol{M}_{\rm p}$ is the Mueller matrix of the polarizer. The polarization properties of a Stokes polarimeter in any state can be conveniently described by the 4×4 Mueller matrix $\boldsymbol{M}_{\rm s}$ which describes the relations between the incident and outgoing Stokes vectors. Because photon detectors are in practice sensitive only to the intensity, only the first row of the Mueller matrix is essential. The modulation of intensity by a 6-state Stokes polarimeter is captured in a 6×4 modulation matrix $\boldsymbol{M}_{\rm mod}$. For each state in Table 1, the corresponding row of the modulation matrix $\boldsymbol{M}_{\rm mod}$ is given by the first row of the Mueller matrix $\boldsymbol{M}_{\rm s}$ of the Stokes polarimeter in that state. Then, we have

$$\boldsymbol{I}_{6\times1} = \tau \boldsymbol{M}_{\rm mod} \boldsymbol{S}_{\rm in}. \tag{15}$$

Here $\boldsymbol{I}_{6\times1}$ is the six light intensities obtained from the modulation states in Table 1. The demodulated Stokes parameters $\boldsymbol{S}_{\rm m} = [I_{\rm m},\ Q_{\rm m},\ U_{\rm m},\ V_{\rm m}]^{\rm T}$ can be directly calculated with

$$\begin{aligned} I_{\rm m} &= \tau \frac{1}{3}\sum_{k=1}^{6} \boldsymbol{M}_{\rm mod}(k,:)\boldsymbol{S}_{\rm in}, \\ Q_{\rm m} &= \tau(\boldsymbol{M}_{\rm mod}(1,:) - \boldsymbol{M}_{\rm mod}(2,:))\boldsymbol{S}_{\rm in}, \\ U_{\rm m} &= \tau(\boldsymbol{M}_{\rm mod}(3,:) - \boldsymbol{M}_{\rm mod}(4,:))\boldsymbol{S}_{\rm in}, \\ V_{\rm m} &= \tau(\boldsymbol{M}_{\rm mod}(5,:) - \boldsymbol{M}_{\rm mod}(6,:))\boldsymbol{S}_{\rm in}. \end{aligned} \tag{16}$$

Equation (16) can be simplified to a simpler form

$$\boldsymbol{S}_{\rm m} = \tau \boldsymbol{X} \boldsymbol{S}_{\rm in}, \tag{17}$$

$$\boldsymbol{X} = \begin{bmatrix} \frac{1}{3}\sum_{k=1}^{6} \boldsymbol{M}_{\rm mod}(k,:) \\ \boldsymbol{M}_{\rm mod}(1,:) - \boldsymbol{M}_{\rm mod}(2,:) \\ \boldsymbol{M}_{\rm mod}(3,:) - \boldsymbol{M}_{\rm mod}(4,:) \\ \boldsymbol{M}_{\rm mod}(5,:) - \boldsymbol{M}_{\rm mod}(6,:) \end{bmatrix}, \tag{18}$$

where $\boldsymbol{X}$ is a normalized 4×4 matrix and named polarization response matrix. It will be a 4×4 unit matrix $\boldsymbol{X}_{\rm ideal}$ if the Stokes polarimeter is ideal,

$$\boldsymbol{X}_{\rm ideal} = \begin{bmatrix} 1 & 0 & 0 & 0 \\ 0 & 1 & 0 & 0 \\ 0 & 0 & 1 & 0 \\ 0 & 0 & 0 & 1 \end{bmatrix}. \tag{19}$$

The $\boldsymbol{X}$ fully expresses the relationship between measured Stokes vector $S_{\rm m}$ and the real Stokes vector $S_{\rm in}$ from an object. It also completely represents the polarization properties of the LCVRs-based Stokes polarimeter. In this situation, the Mueller matrix of LCVR can be obtained by substituting Eqs. (1)–(11) into Eq. (12); then the modulation matrix is obtained by substituting Eq. (12) into Eq. (14); finally, the polarization response matrix is calculated by Eq. (18), which is the polarization model of the LCVRs-based Stokes polarimeter with interference.

4. Simulation and optimization

4.1. Polarization accuracy and polarization response matrix

The difference between $\boldsymbol{X}$ and $\boldsymbol{X}_{\rm ideal}$

$$\Delta\boldsymbol{X} = \boldsymbol{X} - \boldsymbol{X}_{\rm ideal} = \begin{bmatrix} - & - & - & - \\ \varepsilon & \varepsilon/q_{\rm in} & \varepsilon/u_{\rm in} & \varepsilon/v_{\rm in} \\ \varepsilon & \varepsilon/q_{\rm in} & \varepsilon/u_{\rm in} & \varepsilon/v_{\rm in} \\ \varepsilon & \varepsilon/q_{\rm in} & \varepsilon/u_{\rm in} & \varepsilon/v_{\rm in} \end{bmatrix} \tag{20}$$

describes the polarization accuracy of the instrument, where ε is the polarization sensitivity for remote sensing (or S/N), $q_{\rm in}$, $u_{\rm in}$, and $v_{\rm in}$ are the linear polarization degree and circular polarization degree of the object, respectively. The first row is usually neglected as it only affects the intensity but not the polarization. The first column is called the instrumental, and the remaining three columns are called crosstalk among linear polarization and circular polarization. Equation (20) shows that the polarization accuracy of the instrument $\Delta\boldsymbol{X}$ depends on the polarization degree of the object. Most of the observed objects emit partially polarized light and the polarization degree is generally below 0.1, thus $\Delta\boldsymbol{X}$ can be calculated from Eq. (20) by setting $q_{\rm in} = u_{\rm in} = v_{\rm in} = 0.1$. Table 3 lists the requirement of instrumental polarization and crosstalk for different polarization accuracy. It indicates the the instrumental polarization has a tougher requirement than the crosstalk for the partially polarized light.

Table 3. The requirement of instrumental polarization and crosstalk for different polarization accuracy.

Polarization accuracy	Instrumental polarization	Crosstalk
0.01	0.01	0.1
0.001	0.001	0.01
0.0001	0.0001	0.001

4.2. Simulation

For a general optical element without scattering, A, B, C, and D in Eq. (13) can be completely represented by three parameters $t_{\rm p}$, $t_{\rm s}$, and δ in polarization theory as

$$\begin{aligned} A &= |t_{\rm p}|^2 + |t_{\rm s}|^2, \\ B &= |t_{\rm p}|^2 - |t_{\rm s}|^2, \\ C &= 2t_{\rm p}t_{\rm s}\cos\delta, \\ D &= 2t_{\rm p}t_{\rm s}\sin\delta, \end{aligned} \tag{21}$$

where δ is the phase retardation of LCVR. Therefore, it is better to simulate the interference effect as follows.

(i) Calculating the Mueller matrix of LCVR by Eqs. (12), (13), and (21).

(ii) Fitting the three parameters $t_{\rm p}$, $t_{\rm s}$, and δ by Eq. (21) to analyze their relationship with interference.

(iii) Calculating the polarization response matrix $\boldsymbol{X}$ and polarization accuracy $\Delta\boldsymbol{X}$ of the LCVRs-based Stokes polarimeter.

(iv) Analyzing the instrumental polarization and crosstalk over wavelengths.

$$\begin{aligned} &n_1 = 1.5,\ \ d_1 = d_3 = 50\ \text{nm}, \\ &n_{\rm o} = 1.5,\ n_{\rm e} = 1.76,\ d_2 = 5\ \mu\text{m}, \\ &V_{\rm c} = 1.5\ \text{V},\ V_0 = 2.0\ \text{V}, \\ &\theta_0 = 0. \end{aligned} \tag{22}$$

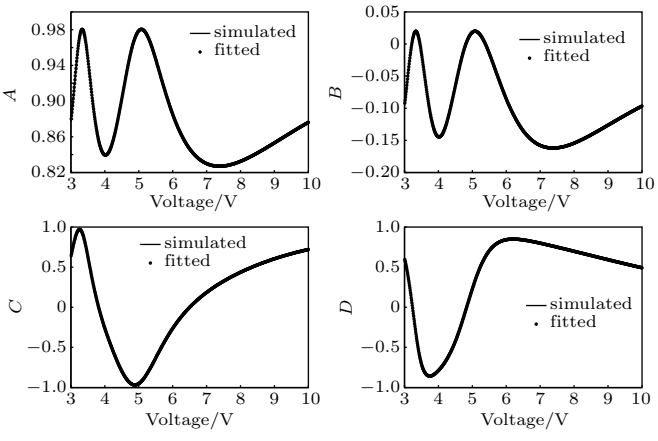


Fig. 5. Mueller matrix of LCVR at 532 nm with interference effect.

Figure 5 displays the simulated Mueller matrix of LCVR at 532 nm with interference. The solid line and dotted line represent the simulated and fitted results, respectively. It can be seen that A, B, C, and D oscillate obviously with the driving voltage due to the interference. Figure 6 gives the corresponding three parameters $t_{\rm p}$, $t_{\rm s}$, and δ fitted. We can find that the

oscillation only comes from t_p, but t_s and δ are not affected by the interference. The variation of t_p with voltages produces a weak polarization like as a polarizer, which induces the instrumental polarization.

Based on the curve of phase retardation δ with voltages in Fig. 6, we can exactly derive the corresponding voltages for 90°, 180°, 270°, and 360° as shown in Table 1. The polarization response matrix $\boldsymbol{X}$ can be calculated with Eqs. (11)–(18) and Table 1. Figure 7 illustrates the relationships between $\Delta\boldsymbol{X}$ and the spectra bandwidth transmitted by the LCVRs-based Stokes polarimeter. The center wavelength is 532 nm. The horizontal axis is the spectra bandwidth $\Delta\lambda$, and the vertical axis is all the elements of $\Delta\boldsymbol{X}$. It is obvious that the instrumental polarization is less than 0.006, and the crosstalk is less than 0.02; their variations with the spectra bandwidth are less than 0.0003 and can be ignored.

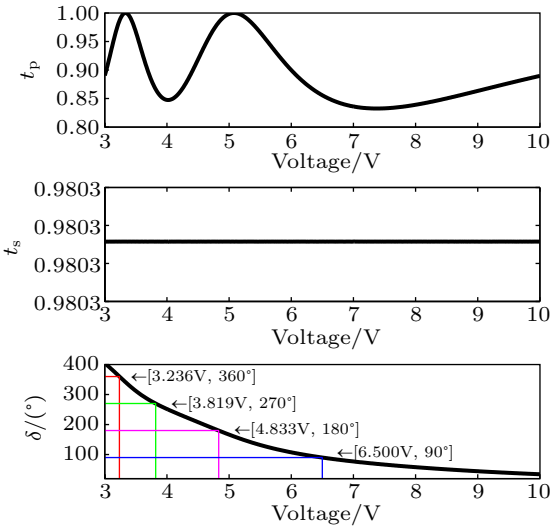


Fig. 6. The fitted t_p, t_s, and δ.

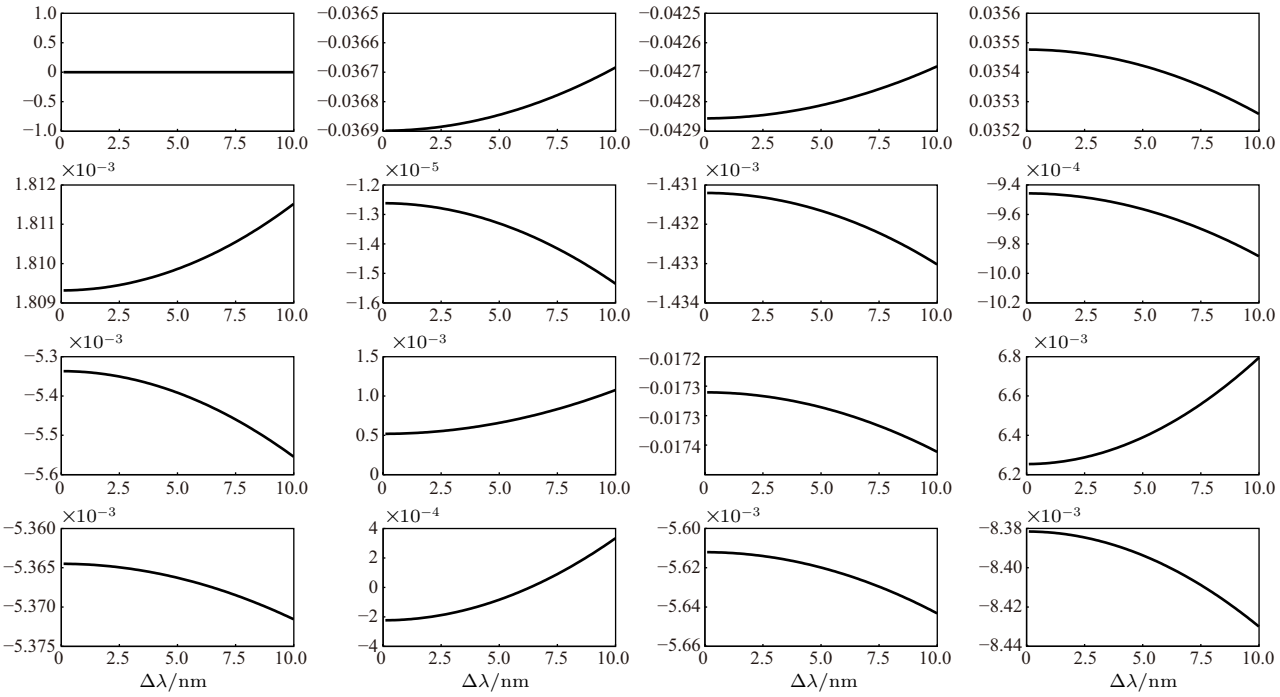


Fig. 7. Polarization accuracy $\Delta\boldsymbol{X}$ vs. the spectra bandwidth of LCVRs-based Stokes polarimeter.

Finally, we can easily obtain $\Delta\boldsymbol{X}$ at different wavelengths by the same method used for 532 nm, as illustrated in Fig. 8. The polarization errors are different in different wavelengths. The instrumental polarization is about 0.01, and the crosstalk is less than 0.025 over the spectral range of 500–600 nm.

In reality, polarization calibration is a necessary step before using any Stokes polarimeter for observations. The polarization calibration accuracy is about 0.01 for the polarization response matrix $\boldsymbol{X}$. It means that, if the polarization accuracy required is higher than 0.01, the interference effect can be ignored. However, if the required polarization accuracy is in the order of 0.01–0.001, we must pay attention to the instrumental polarization induced by the interference. When the required polarization accuracy is better than 0.001, the instrumental polarization and crosstalk have to be taken into account together. Also, the instrumental polarization always has higher requirements than the crosstalk for the weak polarization objects. Thus, it limits the polarization sensitivity of the Stokes polarimeter to 0.01.

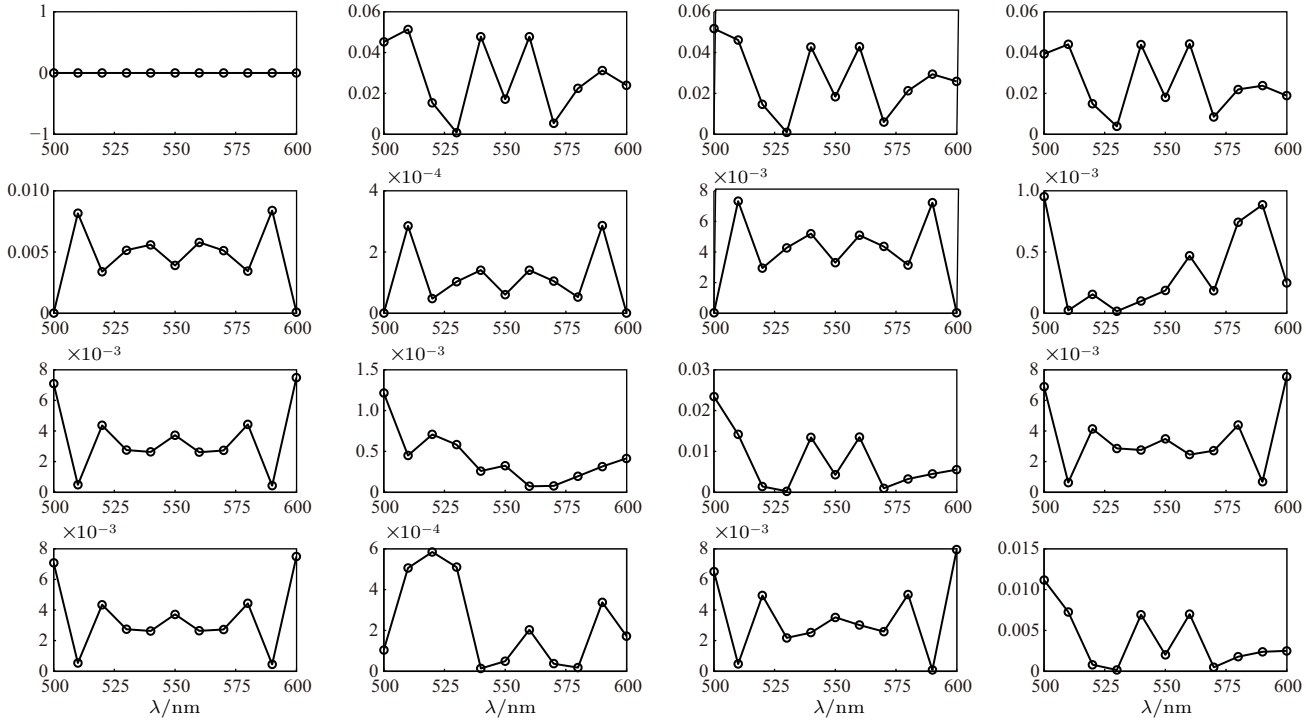


Fig. 8. Polarization accuracy $\Delta \boldsymbol{X}$ vs. wavelengths of LCVRs-based Stokes polarimeter.

4.3. Optimization

The previous simulation shows that the interference in LCVR mainly induces instrumental polarization, which is always more severe than crosstalk. How to minimize or even eliminate the instrumental polarization is an important issue we have to solve for the high accuracy polarization measurements using LCVRs-based Stokes polarimeter. One method is to match the refractive index of ITO and LC, and another one is to choose a particular LC with a small birefringence index. However, both of them are difficult to carry out and also may produce some other problems such as low modulation speed. Here, we propose an optimization method, trying to reduce the instrumental polarization by exact alignment instead of exchanging the LCVRs. By expanding Eqs. (14) and (18), the instrumental polarization of $\boldsymbol{X}$ can be transformed into

$$X_{21} = A_1^{V_{11}}(A_2^{V_{21}} - A_2^{V_{22}}) + B_1^{V_{11}}(C_2^{V_{21}} - C_2^{V_{22}}), \quad (23)$$

$$X_{31} = A_1^{V_{12}}(A_2^{V_{23}} - A_2^{V_{24}}) + B_1^{V_{12}}(C_2^{V_{23}} - C_2^{V_{24}}), \quad (24)$$

$$X_{41} = A_1^{V_{13}}(A_2^{V_{25}} - A_2^{V_{26}}) + B_1^{V_{13}}(C_2^{V_{25}} - C_2^{V_{26}}), \quad (25)$$

where A_1, B_1, C_1, and D_1 are the main parameters of the Mueller matrix of LCVR1; A_2, B_2, C_2, and D_2 are LCVR2's; $V_{11}, V_{12}, V_{13}, V_{21}, V_{22}, V_{23}, V_{24}, V_{25}, V_{26}$ are the driving voltages corresponding to LCVRs' phase retardation, required for polarization modulation. We can see from the above set of equations that LCVR2 always needs two different voltages no matter it is X_{21}, X_{31}, or X_{41} in Eqs. (23)–(25). Also, A_1 is always close to 1 and B_1 is close to 0 from Fig. 5. It means that it is possible to optimize X_{21} to zero by aligning LCVR1's voltage to $B_1^{V_{11}} = 0$ and aligning LCVR2's voltage to $A_2^{V_{21}} - A_2^{V_{22}} = 0$, which is also applicable to X_{31} and X_{41}. In detail, the initial design voltages at 532 nm are shown in Table 4, in which the 2nd and 3rd columns are the initial design results. After considering the interference, V_{11}, V_{12}, V_{13}, V_{22}, V_{24}, and V_{25} can be used as variables to change around the initial values with ± 0.2 V. Thus, we will get the optimized voltages to minimize the instrumental polarization. Table 4 illustrates the optimization results, in which X_{21}, or X_{31}, even X_{41} will be minimized.

Table 4. The driving voltages of LCVR1 and LCVR2 in 6 states. The 2nd and 3rd columns are the initial design results, and the last two columns are the optimized results.

States	V_{LCVR1}/V	V_{LCVR2}/V	V'_{LCVR1}/V	V'_{LCVR2}/V
1	$V_{11} = 3.236$	$V_{21} = 3.236$	$V_{11} = 3.210$	$V_{21} = 3.236$
2	$V_{11} = 3.236$	$V_{22} = 4.833$	$V_{11} = 3.210$	$V_{22} = 4.812$
3	$V_{12} = 6.500$	$V_{23} = 6.500$	$V_{12} = 6.452$	$V_{23} = 6.500$
4	$V_{12} = 6.500$	$V_{24} = 3.819$	$V_{12} = 6.452$	$V_{24} = 3.843$
5	$V_{13} = 3.236$	$V_{25} = 6.500$	$V_{13} = 3.210$	$V_{25} = 6.352$
6	$V_{13} = 3.236$	$V_{26} = 3.819$	$V_{13} = 3.210$	$V_{26} = 3.819$

Figure 9 gives the relationship between the optimized $\Delta \boldsymbol{X}$ and the spectra bandwidth transmitted by the LCVRs-based Stokes polarimeter. Comparing Figs. 9 and 7, we find that the instrumental polarization after optimization is about 0.00025 and far smaller than that of the initial estimation, but the crosstalk and variations with the spectra bandwidth remain the same as before. It implies that the optimization method works well. The optimization method is applied to the whole wavelengths 500–600 nm. Figure 10 shows $\Delta \boldsymbol{X}$ over 500–600 nm, the instrumental polarization is reduced to 0.002, effectively improving the polarization sensitivity of the Stokes polarimeter which is initially limited by the instrumental polarization from interference. We also note that the reduction of the instrument polarization is at the expense of the accuracy of crosstalk in the optimization method. However, the latter can be easily calibrated with high accuracy.

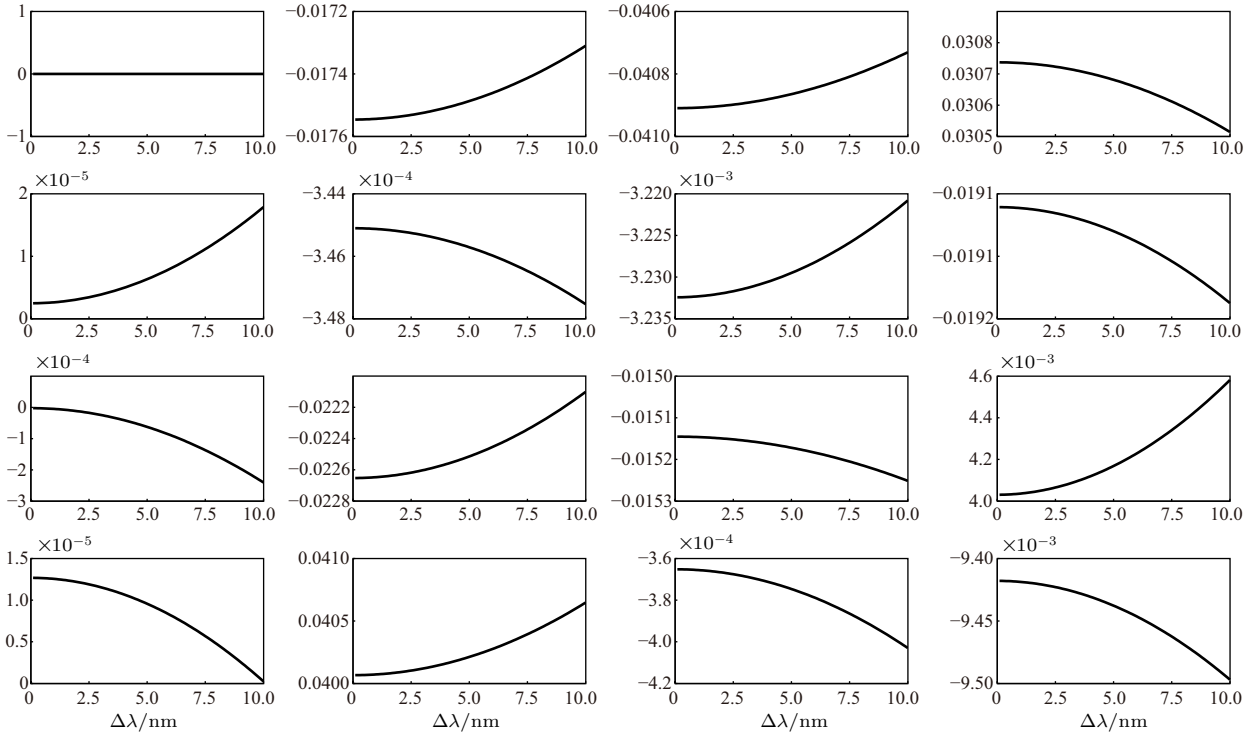


Fig. 9. The polarization accuracy $\Delta \boldsymbol{X}$ vs. the spectra bandwidth of LCVRs based Stokes polarimeter at 532 nm after optimization.

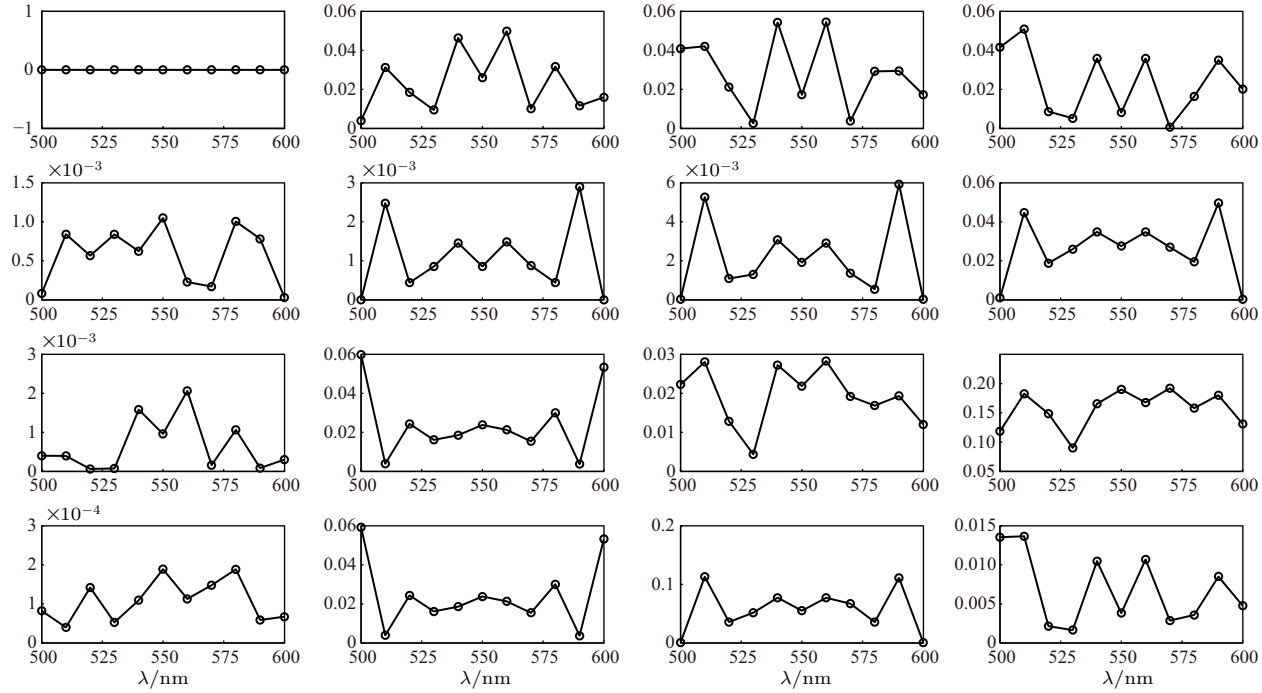


Fig. 10. The polarization accuracy $\Delta \boldsymbol{X}$ of LCVRs-based Stokes polarimeter with wavelengths after optimization.

5. Experiments and analysis

5.1. Measurement and optimization of the LCVRs-based Stokes polarimeter

A LCVRs-based Stokes polarimeter is measured and optimized. The Stokes polarimeter under test is from FMG payload onboard ASO-S satellite.[24,25] A Mueller matrix measurement and calibration system is used to measure both LCVRs and the polarization response matrix $\boldsymbol{X}$ with an accuracy of 0.01.[30,31]

Figure 11 shows the relationship between the measured Mueller matrix of both LCVRs and the derived voltages at 500 nm, where A, B, C, and D are Mueller matrix's four parameters as described in Eq. (21). Then the designed and optimized voltages for both LCVRs can be derived from Fig. 11 according the simulation and optimization methods in Section 4. Finally, the polarization response matrix $\boldsymbol{X}$ of the Stokes

polarimeter can be measured, and the results are plotted in Fig. 12. The blue and red colors indicate the measured results before and after the optimization, respectively. It is obvious that the instrumental polarization decreases significantly after the optimization. In addition, the crosstalk has a variation of about 0.1 over 500–600 nm, thus the polarization calibration is very important before use. It is worth noting that we need to calculate and optimize the driving voltages of both LCVRs at each wavelength according to their Mueller matrix in each wavelength. Therefore, this method is very suitable for imaging-polarization measurement with single wavelength channel. For multi-wavelength channels or spectra-polarization, the calibration and optimization are more complicated.

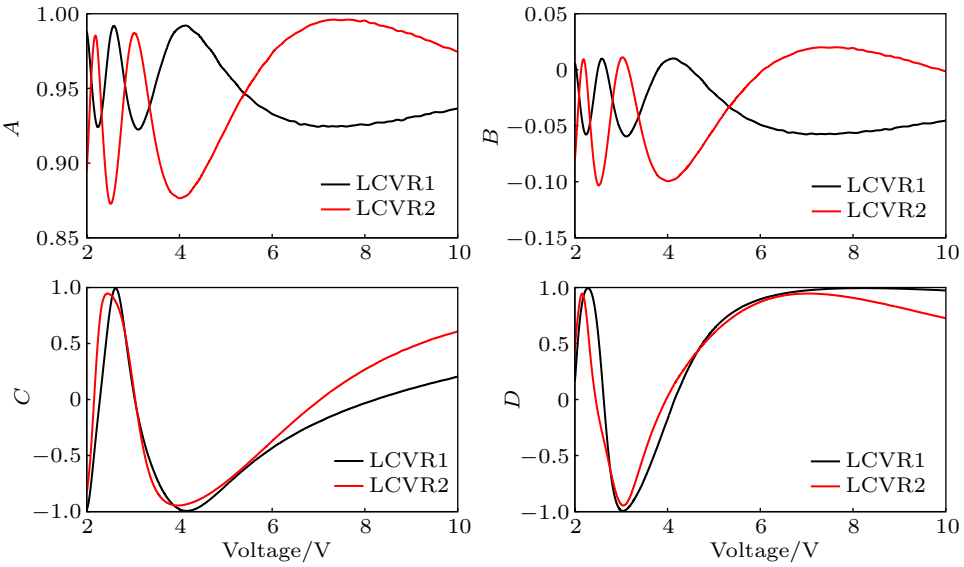


Fig. 11. The measured Mueller matrix of both LCVRs with voltages at 500 nm.

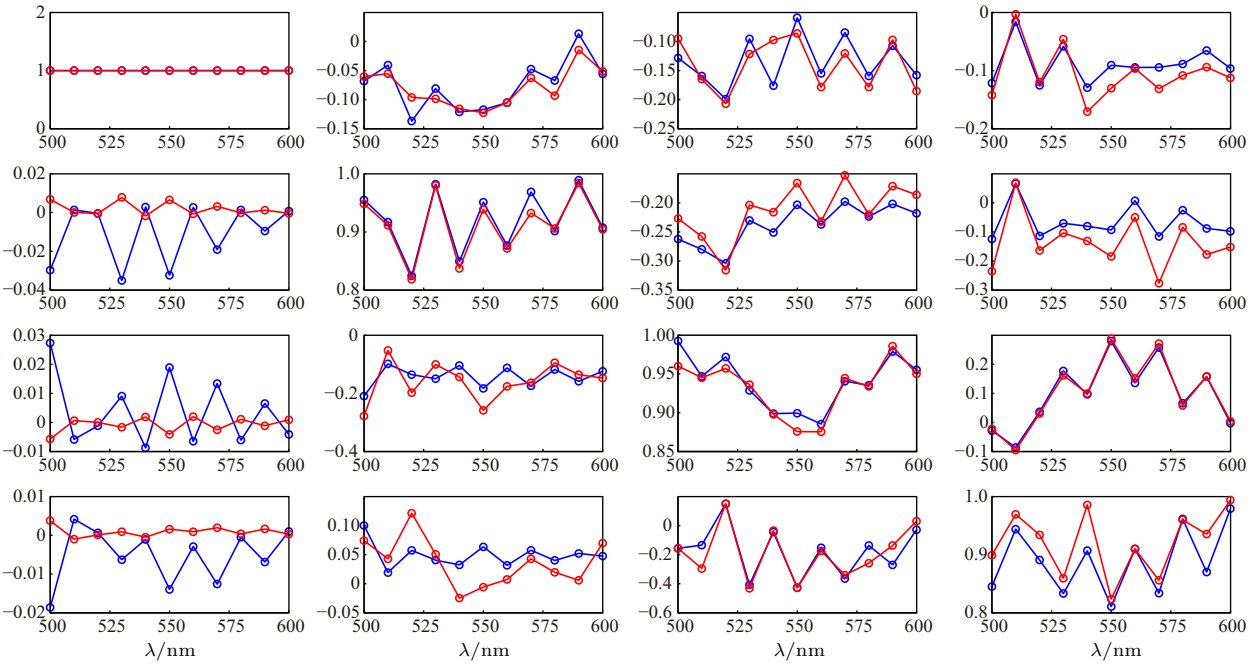


Fig. 12. Polarization response matrix $\boldsymbol{X}$ vs. wavelengths of LCVRs-based Stokes polarimeter. The blue and red colors indicate the measured results before and after the optimization, respectively.

5.2. Accuracy measurement and analysis

An experimental setup is built to verify the effectiveness of the optimization method given above. The unpolarized light source and a diffuse reflectance standard white plate from Labsphere are employed to estimate the measuring accuracy of the LCVRs-based Stokes polarimeter.

The experimental layout is shown in Fig. 13. A combination of the integrating sphere and collimator is used to produce a uniform, polarization-free, and collimated light beam, polarization of which is less than 0.001. Then, the light beam passes

through the LCVRs-based Stokes polarimeter and detected by a fiber spectrophotometer (Ocean Optics USB2000+). Besides, a diffuse reflectance standard white plate is also measured to estimate the measuring accuracy.

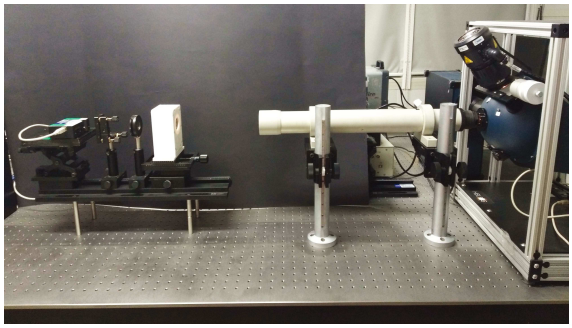


Fig. 13. Experimental setup.

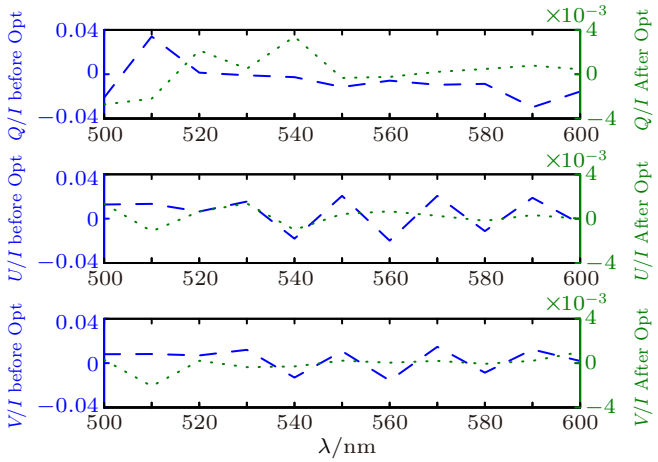


Fig. 14. Stokes parameters of unpolarized light source before and after optimization.

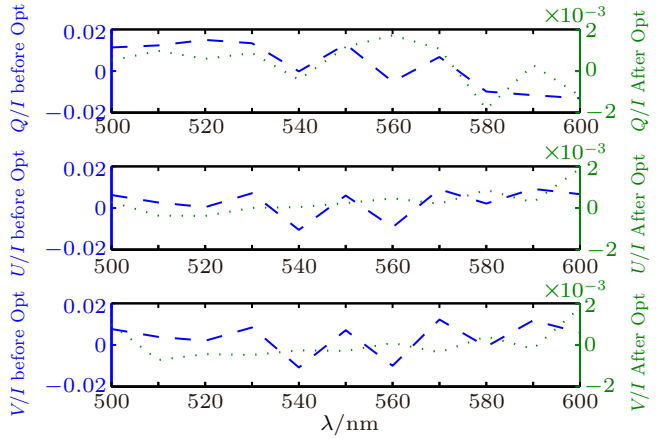


Fig. 15. Stokes parameters of diffuse reflectance standard white plate before and after optimization.

Figures 14 and 15 show the measured Stokes parameters (Q/I, U/I, and V/I) of the unpolarized light source and diffuse reflectance standard white plate vs. wavelengths before and after the optimization. For the unpolarized light source measurement (Fig. 14), the largest instrumental polarization is about 0.04 over 500–600 nm due to the interference before optimization; but after the optimization, the instrumental polarization is less than 0.003. For the diffuse reflectance standard white plate measurement (Fig. 15), the largest instrumental polarization is about 0.02 over 500–600 nm due to the interference before optimization; but after the optimization, the instrumental polarization is less than 0.002. The measurement and simulation have a good agreement with each other.

6. Conclusions

The LCVRs-based Stokes polarimeter is envisaged as a promising novel technique for polarization measurement by space instruments and remote sensing due to the inherent advantage of eliminating the need for conventional rotary polarizing optics and increasing the measuring speed. However, the intrinsic multi-beam interference in LCVRs limits its polarization accuracy by several percent. How to analyze, forecast, optimize, and reduce the influence of the interference effect on the polarization accuracy becomes an urgent issue for the use of LCVRs-based Stokes polarimeter.

Firstly, we proposed a simplified but effective polarization model with interference to simulate the relationship between the interference and polarization accuracy of the LCVRs-based Stokes polarimeter. It is found that the variation of the transmittance of LCVR with its derived voltage is caused by the change of the birefringence index and interference between the ITO film and the liquid crystal, which produces a few percent instrumental polarization. The polarization errors are different in different wavelengths, and also they have no rules to follow. The instrumental polarization is about 0.01, and the cross-talk is less than 0.025 over 500–600 nm. In polarization tolerance analysis, it is known that the instrumental polarization and crosstalk are required to be less than 0.001 and 0.01, respectively if the required polarization accuracy is 0.001. The instrumental polarization always has higher requirements than the crosstalk for the weak polarization sources, and it limits the polarization sensitivity of the Stokes polarimeter to 0.01.

Then, an optimization method was proposed to reduce the instrumental polarization arising due to the interference. The instrumental polarization can be reduced to zero by aligning LCVR1 and LCVR2's voltages and thus effectively improving the polarization sensitivity of the Stokes polarimeter.

Finally, an experimental setup was designed to verify the effectiveness of the optimization. The results show that the instrumental polarization is reduced to 0.002 after the optimization. The simulation and experiment results are in good agreement.

This paper provide an analysis and optimization method of interference effect for LCVRs-based Stokes polarimeter with high polarization accuracy. The optimization method is more effective when the required polarization accuracy is

less than 0.01, especially for LCVRs-based Stokes polarimeter with single wavelength.

References

[1] Clevers J G P W 1999 *ISPRS J. Photogrammetry Remote Sens.* **54** 299
[2] Hagen N and Kudenov M W 2013 *Opt. Eng.* **52** 090901
[3] Curran P J 1994 *Prog. Phys. Geography: Earth Environ.* **18** 247
[4] Demos S G and Alfano R R 1997 *Appl. Opt.* **36** 150
[5] Tyo J S, Goldstein D L, Chenault D B and Shaw J A 2006 *Appl. Opt.* **45** 5453
[6] Du P, Samat A, Waske B, Liu S and Li Z 2015 *ISPRS J. Photogrammetry Remote Sens.* **105** 38
[7] Stenflo J O 1978 *Reports on Progress in Physics* **41** 865
[8] Tinbergen J 2005 *Astronomical polarimetry* (Cambridge: Cambridge University Press) p. 5
[9] Snik F and Keller C U 2013 *Astronomical Polarimetry: Polarized Views of Stars and Planets* (Dordrecht: Springer) pp. 175–221
[10] Ichimoto K, Lites B and Elmore D 2008 *Sol. Phys.* **249** 233
[11] Schou J, Borrero J M and Norton A A 2012 *Sol. Phys.* **275** 327
[12] Hipps K W and Crosby G A 1979 *J. Phys. Chem.* **83** 555
[13] Diner D J, Davis A, Hancock B, Gutt G, Chipman R A and Cairns B 2007 *Appl. Opt.* **46** 8428
[14] Wiehr E 1981 *Astron. Astrophys.* **95** 54
[15] Hou J F 2014 *Proc. SPIE, 9099 Polarization: Measurement, Analysis, and Remote Sensing XI,* p. 909917
[16] Fineschi S, Zangrilli L, Rossi G, Gori L, Romoli M, Corti G, Capobianco G, Antonucci E and Pace E 2005 *Proc. SPIE, 5901 Solar Physics and Space Weather Instrumentation,* p. 59011I
[17] Shaw J A and Pust N J 2006 *Appl. Opt.* **45** 5470
[18] Hou J F, Wijn A G D and Tomczyk S 2013 *Astrophys. J.* **774** 85
[19] PN B, Rust D M, Ha E and Murphy G A 2000 *Proc. SPIE 4014, Airborne Telescope Systems,* p. 214225
[20] Pillet V M, del T I J C, Alvarez-Herrero A, *et al*. 2011 *Sol. Phys.* **268** 57
[21] Barthol P, Gandorfer A, Solanki S K, *et al*. 2011 *Sol. Phys.* **268** 1
[22] Mueller D, Marsden R G, StCyr O C, *et al.* 2013 *Physics* **285** 25
[23] Solanki S K, del T I J C, Woch J, *et al*. 2019 *Astronomy Astrophysics* Accepted
[24] Deng Y Y, Zhang H Y, Yang J F, *et al*. 2019 *RAA* **19** 157
[25] Gan W Q, Ch Z, Deng Y Y, *et al*. 2019 *RAA* **19** 156
[26] Heredero R L, Uribe-Patarroyo N, Belenguer T, Ramos G, Sanchez A, Reina M, Pillet V M and Alvarez-Herrero A 2007 *Appl. Opt.* **45** 689
[27] Hou J F, Wang H F, Wang G, Luo Y Q, Li H W, Zhang Z L, Wang D G and Deng Y Y 2020 *Chin. Phys. B.* **29** 074208
[28] Born M and Wolf E 1999 *Principles of Optics*, 7th edn. (Cambridge: Cambridge University Press) pp. 32–59
[29] Xiao X F and Voelz D 2005 *Proc. SPIE, 5888, Polarization Science and Remote Sensing II,* p. 58881J
[30] Hou J F, Wang D G, Deng Y Y, Sun Y Z and Zhang Z Y 2017 *Chin. Phys. B* **26** 089501
[31] Hou J F, Xu Z, Yuan S, *et al*. 2020 *RAA* **20** 45